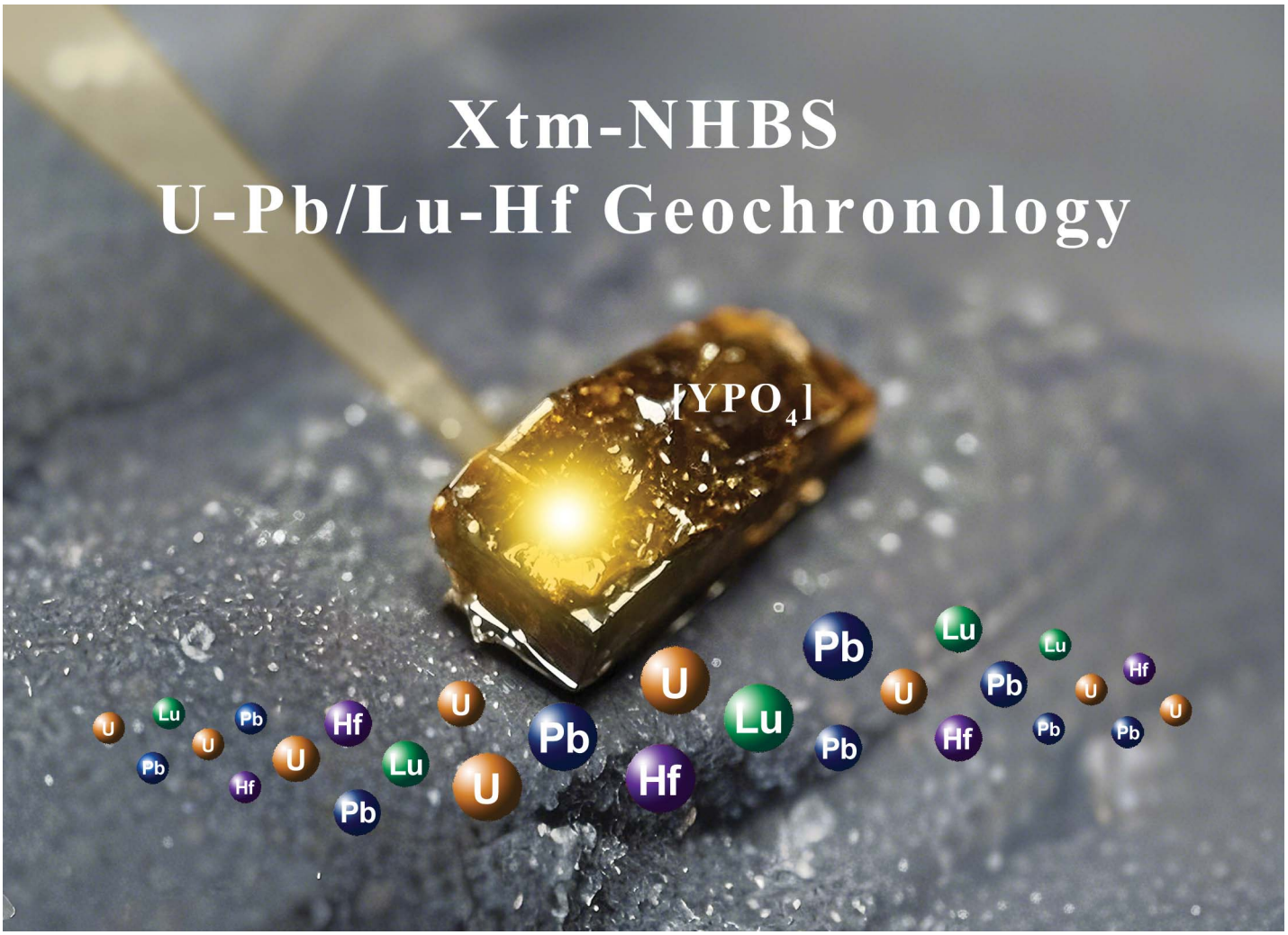

Showcasing research from Professor Prof. Yue-Heng Yang, State Key Laboratory of Lithospheric and Environmental Coevolution, Institute of Geology and Geophysics, Chinese Academy of Sciences, Beijing, P.R.China.

Xenotime Xtm-NHBS: a natural reference material for microbeam U–Pb/Lu–Hf geochronology

Xenotime, a common mineral in various rock types, is typically characterised by high U content with minimal common Pb, making it an excellent candidate for U–Pb dating. However, the limited availability of well-characterised U–Pb xenotime reference materials has hindered its wide application in microanalysis. We present the characterisation of Xtm-NHBS xenotime as a reference material for *in situ* U–Pb/Lu–Hf geochronology, using LA-ICP-MS, LA-ICP-MS/MS and ID-TIMS techniques, to assess its feasibility as a primary U–Pb/Lu–Hf reference material.

Image reproduced by permission of Yueheng Yang from *J. Anal. At. Spectrom.*, 2025, **40**, 931.

As featured in:

See Yueheng Yang *et al.*, *J. Anal. At. Spectrom.*, 2025, **40**, 931.

ROYAL SOCIETY OF CHEMISTRY

rsc.li/jaas

Registered charity number: 207890

JAAS

ROYAL SOCIETY OF CHEMISTRY

TECHNICAL NOTE

Cite this: *J. Anal. At. Spectrom.*, 2025, **40**, 931

Xenotime Xtm-NHBS: a natural reference material for microbeam U–Pb/Lu–Hf geochronology†

Shuya Zhang,[ab] Yueheng Yang, *[ab] Shitou Wu, [ab] Jiarun Tu,[c] Lei Xu,[ab] Hao Wang,[ab] Liewen Xie, [ab] Chao Huang, [ab] Jinhui Yang[ab] and Fuyuan Wu[ab]

Xenotime is a common mineral found in various rock types, including magmatic, metamorphic, and sedimentary rocks. It is typically characterised by high uranium (U) and thorium (Th) content, with minimal common lead (Pb), making it an excellent candidate for U–Pb dating. However, the limited availability of well-characterised U–Pb xenotime reference materials (*e.g.*, BS-1 and MG-1) has hindered its wide application in microanalysis. With the rapid advancements in laser ablation inductively coupled plasma tandem mass spectrometry (LA-ICP-MS/MS), the demand for xenotime reference materials, particularly for *in situ* Lu–Hf geochronology, has grown significantly. This study presents the characterisation and assessment of Xtm-NHBS xenotime as a potential primary U–Pb reference material for microanalysis. U–Pb isotopic analyses were performed using isotope dilution thermal ionisation mass spectrometry (ID-TIMS) and laser ablation quadrupole/sector field inductively coupled plasma mass spectrometry (LA-Q/SF-ICP-MS) to evaluate the homogeneity of gem-quality xenotime crystals. The ID-TIMS analysis yielded a $^{206}Pb/^{238}U$ age of 498.7 ± 0.4 Ma (2s, $n = 5$, MSWD = 0.99). The $^{206}Pb/^{238}U$ ages obtained *via* LA-Q/SF-ICP-MS across multiple analytical sessions were consistent with the ID-TIMS results, demonstrating homogeneity with ~1% precision using *in situ* techniques. Additionally, the ages of BS-1, MG-1, and XN Datas can be reproduced by LA-SF-ICP-MS when calibrated against the Xtm-NHBS crystal as a primary reference material. Meanwhile, the Lu–Hf age of this crystal by LA-ICP-MS/MS is also presented in this study. The newly characterised natural Xtm-NHBS xenotime offers a significant contribution to advancing *in situ* U–Pb/Lu–Hf geochronology, enhancing both accuracy and precision in microanalytical applications.

Received 13th January 2025
Accepted 3rd March 2025

DOI: 10.1039/d5ja00013k

rsc.li/jaas

1. Introduction

Xenotime (YPO_4) is a common accessory mineral found in various rock types, including pelitic metamorphic rocks, peraluminous granites, and siliciclastic sedimentary rocks. It is an ideal candidate for U–Pb dating due to its high uranium (U) content and negligible levels of common lead (Pb).[1] Typically, xenotime U–Pb geochronology requires high spatial resolution instrumentation (*e.g.*, *in situ* dating) to account for its well-documented textural complexities.[2–4] Historically, high spatial resolution U–Pb dating of xenotime has been performed using Secondary Ion Mass Spectrometry (SIMS), primarily with the SHRIMP-II instrument.[5–7] More recently, the SIMS Cameca 1280 [8] and especially Laser Ablation Inductively Coupled Plasma Mass Spectrometry (LA-ICP-MS) have also been utilised for *in situ* U–Pb dating.[1,9,10]

The availability of matrix-matched reference materials is crucial for calibration and quality control in *in situ* isotopic methodologies.[7,11–15] *In situ* U–Pb measurements mainly rely on external calibrations, typically achieved using the standard-bracketing method.[16–18] With the growing number of LA-(MC)-ICP-MS instruments, U–Pb xenotime reference materials (*e.g.*, BS-1 and MG-1) developed for SIMS over more than two decades ago are insufficient to meet the current demand for rapid microanalysis.[4,19] Furthermore, the demand for reliable reference materials has increased due to the popularity of LA-ICP-MS U–Pb geochronology, which consumes significantly larger amounts of reference material compared to SIMS.[15] For instance, BS-1 and MG-1, originally developed for SIMS in 2004, are now largely unavailable for LA-ICP-MS laboratories.[1,9,10,15]

Recent efforts, such as the development of XN Datas xenotime reference materials, require interlaboratory further validation to assess their homogeneity.[15] Meanwhile, the rapid development of tandem ICP-MS paired with laser ablation (LA-ICP-MS/MS) has increased demand for xenotime reference materials suited for *in situ* Lu–Hf dating.[20–22] Consequently,

[a]*State Key Laboratory of Lithospheric and Environmental Coevolution, Institute of Geology and Geophysics, Chinese Academy of Sciences, Beijing, 100029, China. E-mail: yangyueheng@mail.iggcas.ac.cn*

[b]*College of Earth and Planetary Science, University of Chinese Academy of Sciences, Beijing, 100049, China*

[c]*Tianjin Center, China Geological Survey, Tianjin 300170, China*

† Electronic supplementary information (ESI) available. See DOI: https://doi.org/10.1039/d5ja00013k

there is an urgent need for the development of new xenotime reference materials tailored for microbeam U–Pb/Lu–Hf geochronology.

In this study, we present the characterisation of Xtm-NHBS xenotime as a reference material for *in situ* U–Pb/Lu–Hf geochronology, using LA-(Q, SF)-ICP-MS, LA-ICP-MS/MS and ID-TIMS techniques. The primary objectives are (i) to evaluate the elemental and isotopic homogeneity of the material and (ii) to assess its feasibility as a primary U–Pb/Lu–Hf reference material.

2. Experimental

The experiments were conducted on fragments from four single-grain specimens: BS-1, MG-1, XN Datas, and Xtm-NHBS. Xenotime crystal fragments and individual crystals were mounted in epoxy resin and polished to expose the interiors of the samples. Transmitted and reflected light photomicrographs were obtained to document the xenotime specimens. U–Pb age measurements were performed using ID-TIMS and LA-Q/SF-ICP-MS techniques at two laboratories: the Tianjin Centre of the China Geological Survey (TJ-CGS) in Tianjin and the State Key Laboratory of Lithospheric and Environmental Coevolution (SKLLEC) at the Institute of Geology and Geophysics, Chinese Academy of Sciences (IGG-CAS) in Beijing.

2.1 Sample descriptions

BS-1 and MG-1 crystal fragments were provided by Dr John Aleinikoff, originally sourced from Dr Miguel Basei at the University of São Paulo, Brazil. These crystals are derived from metamorphic host rocks, although their precise genesis remains unknown. BS-1 originates from Bahia State, while MG-1 comes from Ouro Preto in Minas Gerais State.[7] BS-1 has an ID-TIMS $^{206}Pb/^{238}U$ age of 508.9 ± 0.3 Ma (1σ) and a $^{207}Pb/^{206}Pb$ age of 505.5 ± 0.6 Ma (1σ).[19] For MG-1, the ID-TIMS ages are near-concordant, with a $^{206}Pb/^{238}U$ age of 490.0 ± 0.3 Ma (1σ) and a $^{207}Pb/^{206}Pb$ age of 491.8 ± 0.6 Ma (1σ).[19] Both samples have independent ID-TIMS U–Pb analyses and are used as primary reference materials. Comprehensive descriptions of the original BS-1 and MG-1 crystals are detailed by Fletcher *et al.*[19] and Aleinikoff *et al.*[6]

The XN Datas crystal fragments were provided by Dr Vasconcelos and donated by the Museu de Ciência e Tecnologia da Escola de Minas de Ouro Preto, Minas Gerais, Brazil.[15] These samples likely originated from quartz veins near the cities of Datas and Diamantina, located in the southern Espinhaço range. Regional studies and mineral geochemical analyses suggest that these quartz veins are related to multiple episodes of devolatilisation during folding and metamorphism around 500 Ma. XN01 Datas has an ID-TIMS $^{206}Pb/^{238}U$ age of 513.4 ± 0.5 Ma (1σ) and a $^{207}Pb/^{206}Pb$ age of 514.8 ± 1.4 Ma (1σ).[15] The ID-TIMS ages for XN02 Datas are near-concordant, with a $^{206}Pb/^{238}U$ age of 515.4 ± 0.2 Ma (1σ) and a $^{207}Pb/^{206}Pb$ age of 517.0 ± 2.0 Ma (1σ).[15] A reference $^{206}Pb/^{238}U$ age of 514 Ma has been adopted for XN Datas as a secondary reference material for data quality in this study.

The Xtm-NHBS xenotime sample was obtained from the Mineralogical Research Co. and is reported to originate from Novo Horizonte, Bahia State, Brazil. The brown xenotime crystals studied in this work likely come from the same region and were probably formed in similar hydrothermal quartz vein deposits. The crystals vary from euhedral to subhedral forms, occurring as centimetre-sized, gem-quality metacrysts that are relatively abundant and suitable for distribution to LA-ICP-MS laboratories (Fig. 1). However, individual metacrysts from these deposits have not been previously characterised. This study focuses on assessing their chemical homogeneity using *in situ* techniques to evaluate their suitability as U–Pb/Lu–Hf reference materials, followed by high-precision TIMS U–Pb geochronology.

2.2 Major and trace element analysis

Major element analysis and backscattered electron (BSE) imaging were conducted using a Cameca SX Five electron microprobe. The operating conditions included a beam current of 3×10^{-8} A, an acceleration voltage of 15 kV, and a beam diameter of 5 μm. The peak counting time was set to 20 seconds for all elements, with a background counting time of 10 seconds on both high- and low-energy background positions. The rare earth element (REE) abundances were calibrated against synthetic REE phosphate standards, while U and Th calibrations were carried out using U oxide and Th oxide standards. The minerals were routinely analysed for Y, P, Si, Ca, Nd, Sm, Gd, Tb, Dy, Ho, Er, Tm, Yb, Lu, Pb and Th. Peak and background positions for each element were carefully selected from EPMA scans of the three xenotime reference materials: BS-1, MG-1, and XN Datas.

Trace element measurements were performed using an Agilent 8900 Quadrupole Q-ICP-MS, coupled with an ESI NWR 193 nm ArF excimer laser, at Volatile Laboratory, IGG-CAS. The laser fluence, spot size, and repetition rate were set to 3 J cm^{-2}, 44 μm, and 6 Hz, respectively. The He carrier gas flows were optimised by ablating NIST 610 glass to achieve maximum signal intensity for $^{238}U^+$ while maintaining a ThO^+/Th^+ ratio of <0.5% and a U/Th ratio of ~1. The ARM-2/BCR-2G reference material was analysed alongside every ten samples. External calibration was conducted relative to ARM-2 glass, using the values recommended by Wu *et al.*,[23] with internal standardisation based on Y content. The accuracy and precision of the analyses were assessed using BCR-2G, with the results consistently better than 10% combined. Trace element data reduction was carried out using Iolite 4 software.

2.3 ID-TIMS U–Pb measurement

Xenotime chips were dated using ID-TIMS U–Pb geochronology at Isotope Laboratory, TJ-CGS. Milli-Q water (18.2 MΩ cm^{-1} at 25 °C) from Millipore (Elix-Millipore, USA) was used for all sample chemical preparations. Concentrated hydrochloric, nitric, and hydrofluoric acids (BV-III grade) from the Beijing Institute of Chemical Reagents were purified twice using a Savillex™ DST-1000 Teflon apparatus sub-boiling distillation system (Minnetonka, MN, USA). All chemical procedures were

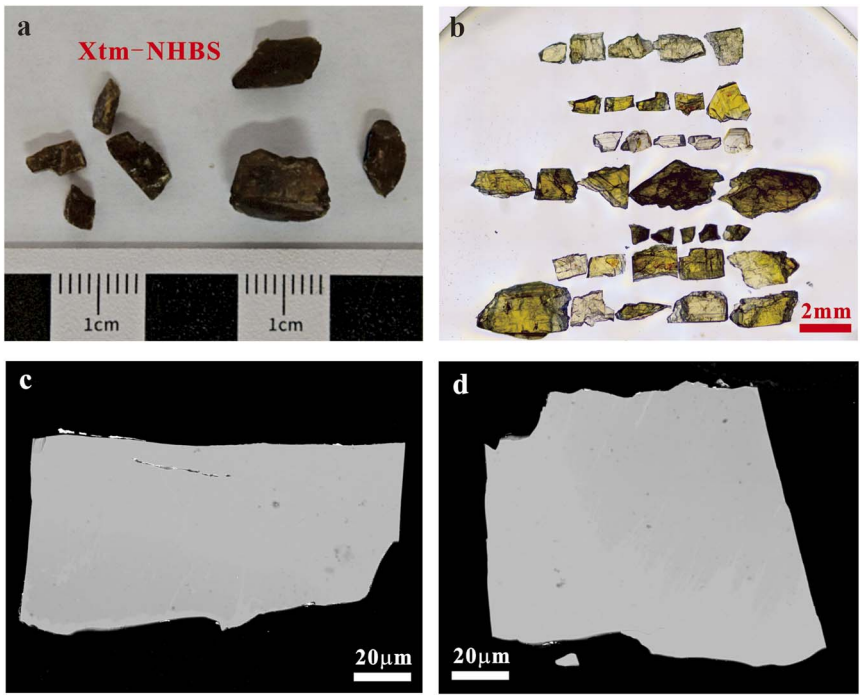

Fig. 1 The grain photograph and backscatter electron (BSE) image are shown for xenotime Xtm-NHBS crystals in this work. (a) The crystals are brown in color and have subhedral shapes. (b) Crystal fragments for the epoxy mounts, showing a brownhoney color. (c) and (d) BSE images of Xtm-NHBS xenotime chips for laser measurements.

carried out in Class 100 fume hoods located within a suite of Class 1000 over-pressured clean rooms. The analytical techniques for sample digestion, column chemistry, and mass spectrometry are described in detail by Tu *et al.*[24]

Xenotime chips were handpicked under a microscope to avoid those with inclusions or fractures. Approximately 0.06–0.08 mg of xenotime chips was weighed and soaked in ultrapure anhydrous alcohol, 7 M HNO_3, and 2 M HCl for 3, 4, and 12 hours, respectively, to remove surface contamination. HNO_3 and HCl leaching were performed on a hot plate at 80 °C. Following this, 1 mL of concentrated HCl was added to the xenotime, which was then completely digested after 72 hours in a temperature-controlled oven at 205 °C.[25] The digested sample solutions were dried to a precipitate, and the redissolved solution was divided into two aliquots. One aliquot (~70%) was used for Pb isotopic ratio measurement, and the other (~30%) for U–Pb concentration measurement after adding four drops (~60 mg) of a mixed ^{208}Pb–^{235}U spike. The solution aliquots were weighed, evaporated to dryness on a hot plate at 125 °C, and then re-dissolved in 0.5 mL of a solution consisting of two parts 1 M HCl and one part 1 M HBr. Pb and U were separated using AG1-X8 anion exchange resin. The purified Pb and U fractions were loaded onto outgassed single rhenium filaments with H_3PO_4 and silica gel, respectively, and then dried at a low temperature.

U–Pb isotopic ratios were measured on a Triton TIMS. Pb isotopic ratios were measured at temperatures of 1250–1440 °C and its cup configuration was set as center cup C to collect ^{204}Pb, H1 to collect ^{206}Pb, H2 to collect ^{207}Pb, and H3 to collect ^{208}Pb. The U isotope ratio was measured as $^{235}UO_2^+$ and $^{238}UO_2^+$ at a current of 2800–3300 mA, and its cup configuration was set as center cup C to collect $^{235}UO_2$ and H2 to collect $^{238}UO_2$. Except that ^{204}Pb was collected using an electron multiplier, other isotopes were collected using a Faraday cup. Uranium reference material U500 and Pb reference material SRM 982 were used to correct for mass discrimination. The total procedural blank for lead and uranium during the ID-TIMS experiment was 13 pg and 1 pg, respectively. For common Pb monitoring, the ^{204}Pb signal was employed, and corrections were made based on the blank and its initial Pb composition, as stipulated by the Stacey–Kramers model.[26,27]

2.4 *In situ* U–Pb measurement

2.4.1 LA-Q-ICP-MS. *In situ* U–Pb analyses were conducted using an Agilent 7500a quadrupole Q-ICP-MS coupled with a GeoLas HD 193 nm ArF excimer laser at MC-ICP-MS Laboratory, IGG-CAS.[1] The laser fluence, spot size, and repetition rate were set to 3 J cm^{-2}, 32 μm, and 6 Hz, respectively. The He carrier gas flows were optimised by ablating NIST 610 glass to achieve maximum signal intensity for $^{238}U^+$ while maintaining a ThO^+/Th^+ ratio of <0.5% and a U/Th ratio of ~1. Each analysis included approximately 20–30 seconds of background acquisition followed by 50 seconds of data acquisition, during which ^{202}Hg, $^{204}(Pb + Hg)$, ^{206}Pb, ^{207}Pb, ^{208}Pb, ^{232}Th, and ^{238}U were measured with dwell times of 10, 10, 20, 20, 10, 20, and 20 ms, respectively. Data reduction was carried out offline using Iolite 4 software. BS-1 xenotime was employed as the primary external standard to correct for background, elemental/isotopic fractionation, and instrumental drift, while MG-1 or XN Datas

xenotime was analysed alternately as an unknown sample during analytical sessions.

2.4.2 LA-SF-ICP-MS. *In situ* U–Pb isotope analyses were performed using an Element XR SF-ICP-MS coupled with a GeoLas HD 193 nm ArF excimer laser at MC-ICP-MS Laboratory, IGG-CAS.[7,28,29] The system was optimised to achieve low oxide production rates ($ThO^+/Th^+ < 0.5\%$), low double-charged ions ($Ca^{2+}/Ca^+ < 1.0\%$), and robust plasma conditions (U^+/Th^+ ranging from 0.95 to 1.05) using ARM-1, while maximising signal-to-noise ratios. Isotopes including ^{202}Hg, $^{204}(Pb + Hg)$, ^{206}Pb, ^{207}Pb, ^{208}Pb, ^{232}Th, and ^{238}U were analysed by cycling the electrostatic analyser with a static magnet mass. The laser beam diameter was 10 μm, and the laser repetition rate was 2 Hz, with an average on-sample fluence of approximately 3 J cm^{-2}. Each spot measurement consisted of approximately 15 seconds of background acquisition followed by 20 seconds of data acquisition, consistent with procedures for zircon. The raw data were exported and processed offline using Iolite 4 software to calculate U–Pb ages. BS-1 xenotime was used as the primary U–Pb reference material, with systematic downhole fractionation corrections applied, while MG-1 or XN Datas xenotime served as the secondary reference material.

2.4.3 LA-Q-ICP-MS. *In situ* U–Pb analyses were conducted using an Agilent 8900 quadrupole Q-ICP-MS/MS coupled with an ESI NWR 193 nm ArF excimer RESOlution SE laser at Volatile Laboratory, IGG-CAS. After a warmup of the 8900 ICP-MS/MS and connection with the laser ablation system, the instrument is first tuned for robust plasma conditions by optimizing laser and ICP-MS/MS settings, monitoring $^{232}Th^{16}O^+/^{232}Th^+$ ratios (always ≤0.5%) and $^{238}U^+/^{232}Th^+$ ratios (always between 0.90 and 1.10) while ablating NIST SRM 610 in line scan mode. The analyses were performed using a spot diameter of 38 μm, a repetition rate of 5 Hz, and a laser fluence of 3.0 J cm^{-2}. Each analysis included 20 s of background acquisition and 50 s of data acquisition, with a total dwell cycle of 227 ms, including a 10 ms dwell time for ^{206}Pb, 30 ms dwell time for ^{207}Pb, 15 ms dwell time for ^{208}Pb, 10 ms dwell time for ^{232}Th, and 10 ms dwell time for ^{238}U. Data reduction was performed offline using Iolite 4 software. BS-1 xenotime was employed as the primary external standard for correcting background, elemental/isotopic fractionation, and instrumental drift, while MG-1 or XN Datas was analysed alternately as an unknown sample during analytical sessions.

2.5 *In situ* Lu–Hf measurement

In situ Lu–Hf dating of xenotime was carried out using a Photon Machines Analyst G2 193 nm ArF excimer LA system coupled to an iCAP triple-quadrupole (TQ) ICP-MS/MS. The method followed was that by Wu *et al.*[22] and a brief description was given. The ICP-MS/MS conditions were first optimized in single quadrupole and no-gas mode to tune the system for robust plasma conditions (U/Th = 1.00–1.05, using NIST SRM 610) and to minimize oxide interference (ThO/Th < 0.5%). The instrument was then switched to TQ mode with NH_3 as the reaction gas for lens tuning (*e.g.*, the collision reaction cell entry lens) to maximize the sensitivity for the Hf reaction products while maintaining low Lu and Yb reaction rates at a mass shift of +82.[21] High-purity (99.999%) NH_3 was used as the reaction gas because it's more efficient than the pre-mixed NH_3–He gas. A small amount of N_2 (4.0 mL min^{-1}) was added to the carrier gas after the sample chamber to enhance the sensitivity.

The reaction product $^{176}Hf(NH)(NH_2)(NH_3)_3^+$ (expressed as $^{(176+82)}Hf$) was measured to separate ^{176}Hf from ^{176}Lu and ^{176}Yb. To avoid any potential memory effect of Lu-based NH_3 reaction products, which may interfere with Hf reaction products (*e.g.*, $^{(175+83)}Lu$ on $^{(176+82)}Hf$), a short dwell time (1 ms) for ^{175}Lu was applied. The diameter of the laser spot was ∼50 μm with a laser repetition ratio of 10 Hz and a fluence of ∼4 J cm^{-2}, depending on Lu and Hf contents. ^{175}Lu was monitored as a proxy for ^{176}Lu, and the present-day $^{176}Lu/^{175}Lu$ ratio of 0.02655 was used to calculate ^{176}Lu contents from ^{175}Lu contents. Reference materials (XN Datas and NIST SRM 610) were used as the primary reference materials to correct for instrumental drift and matrix independent fractionation. BS-1 and MG-1 were measured as unknown samples for quality monitoring during analytical sessions.[30,31]

The Lu–Hf isotopic data were processed using Iolite version 4 with a new DRS.[30,31] Iolite was used to calculate gas blank-corrected intensities and raw ratios (*e.g.*, $^{176}Lu/^{176}Hf$) and their uncertainties. All other calculations were carried out using the *in situ* Lu–Hf dating 2 DRS, including elemental fractionation, matrix bias (between NIST SRM 610 and xenotime), common Hf contents, and corrections for the potential interference of $^{(176+82)}Lu$ and $^{(176+82)}Yb$ on $^{(176+82)}Hf$. Lu–Hf ages of xenotime were calculated using IsoplotR35.[22,30,31]

Table 1 The major (wt%) elements of Xtm-NHBS, BS-1, MG-1 and XN Datas ($n = 10$) by electron probe microanalysis (EPMA)

Samples	Y_2O_3	SiO_2	P_2O_5	CaO	ThO_2	PbO	Nd_2O_3	Sm_2O_3	Gd_2O_3	Dy_2O_3	Ho_2O_3	Er_2O_3	Tm_2O_3	Yb_2O_3	Lu_2O_3	Total	ΣREE
Xtm-NHBS	46.94	0.23	33.02	0.01	0.25	0.38	0.18	0.49	3.12	5.71	1.08	3.98	0.57	3.68	0.30	99.96	19.52
SD	0.69	0.04	0.31	0.01	0.09	0.04	0.06	0.13	0.52	0.15	0.07	0.14	0.02	0.19	0.04	0.50	
BS-1	45.31	0.26	33.08	0.01	0.23	0.36	0.23	0.66	3.63	5.74	1.04	3.81	0.54	3.49	0.31	98.75	19.00
SD	0.58	0.06	0.25	0.01	0.16	0.03	0.07	0.21	0.45	0.23	0.08	0.12	0.03	0.051	0.06	0.45	
MG-1	48.17	0.11	34.43	0.01	0.11	0.40	0.26	0.73	4.92	4.98	0.79	2.10	0.26	1.17	0.07	98.57	10.99
SD	4.60	0.03	0.75	0.01	0.06	0.06	0.04	0.38	3.57	0.84	0.08	0.35	0.03	0.22	0.03	2.28	
XN Datas	43.15	0.11	34.06	0.01	0.04	0.38	0.19	0.48	3.23	5.69	1.07	4.32	0.63	4.66	0.54	98.65	22.40
SD	0.48	0.02	0.25	0.01	0.02	0.03	0.04	0.032	0.14	0.12	0.04	0.08	0.03	0.28	0.03	0.41	

Table 2 Average trace element concentrations (μg g^{-1}) of Xtm-NHBS, BS-1, MG-1 and XN Datas determined by LA-Q-ICP-MS[a]

Samples	*n*	La	Ce	Pr	Nd	Sm	Eu	Gd	Tb	Dy	Ho	Er	Tm	Yb	Lu	Hf	Pb	Th	U	Th/U	Eu/Eu	$(La/Gd)_N$	$(Gd/Lu)_N$
Xtm-NHBS	30	1.87	38.8	28.3	531	1822	831	12 354	3466	30 987	6610	18 873	2308	12 573	1131	2.00	39.8	991	129	7.43	0.40	8631	1.37
SD		0.57	9.1	4.4	58	275	136	1542	315	1627	207	595	103	763	56	0.20	20.3	554	65	0.65	0.02	2298	0.21
RSD (%)		30.6	23	15.4	11	15	16	12	9.1	5.3	3.1	3.2	4.5	6.1	4.9	9.82	51.0	56	51	8.73	5.42	27	15.1
BS-1	29	3.27	70	48	914	3642	1424	18 132	4131	32 711	6595	18 452	2250	12 496	1195	2.14	61.27	1989	195	10.0	0.44	6797	1.90
SD		0.36	8	6	92	349	88	848	123	661	59	295	74	622	95	0.08	14.73	647	46	1.56	0.00	603	0.18
RSD (%)		10.89	12	12	10	10	6.20	4.68	2.98	2.02	0.90	1.60	3.28	4.97	7.91	3.82	24.04	33	24	15.7	1.0	8.9	9.5
MG-1	44	6.98	57.4	58.5	1170	3336	1905	18 282	3326	24 313	4533	9831	823	3347	262	1.39	172	777	681	1.13	0.60	3233	8.81
SD		0.67	4.29	4.06	90	305	153	1709	264	1268	84	167	31	221	36	0.18	24	198	109	0.23	0.03	648	1.05
RSD (%)		9.43	7.33	6.83	7.6	9.3	8.1	9.7	8.3	5.4	1.9	1.7	3.8	6.6	14	14	13	24	15	20.9	4.57	22	12.11
XN Datas	30	2.76	53.4	39.1	744	2435	1780	14 463	3753	32 697	7114	21 330	2760	17 201	2146	2.00	163	398	605	0.64	0.72	6451	0.84
SD		0.37	6.2	4.1	71	256	127	844	167	937	97	354	78	766	120	0.12	41	149	164	0.10	0.03	624	0.09
RSD (%)		13.5	11.6	10.4	9.5	10.5	7.14	5.83	4.44	2.87	1.36	1.66	2.83	4.46	5.61	6.01	25	37	27	15.29	3.67	9.67	10.5

[a] Eu/Eu, (La/Gd)N, and (Gd/Lu)N were calculated using normalized values by the chondritic concentrations of McDonough and Sun (1995).[33]

Table 3 U–Pb isotopic result of Xtm-NHBS xenotime using ID-TIMS in this work[a]

			Content (ppm)			Isotope ratio								Age (Ma)						
Sample	No.	Weight/g	Pb	Pb_c	U	$^{206}Pb/^{204}Pb$	Err%	$^{206}Pb/^{238}U$	Err%	$^{207}Pb/^{235}U$	Err%	$^{207}Pb/^{206}Pb$	Err%	$^{206}Pb/^{238}U$	1s	$^{207}Pb/^{235}U$	1s	$^{207}Pb/^{206}Pb$	1s	Rho (7/5–6/8)
Xtm-NHBS	1	0.00030	45.4	0.3	206.1	1290.9	0.03	0.080383	0.10	0.63366	0.13	0.05717	0.06	498.4	0.5	498.4	0.6	497.2	1.4	0.873
	2	0.00034	39.2	0.3	178.4	1234.1	0.03	0.080490	0.10	0.63410	0.12	0.05714	0.06	499.0	0.5	498.6	0.6	495.8	1.4	0.852
	3	0.00027	43.7	0.4	198.4	1132.3	0.02	0.080512	0.08	0.63417	0.11	0.05713	0.07	499.2	0.4	498.7	0.6	495.5	1.6	0.781
	4	0.00041	45.1	0.3	204.9	1651.3	0.02	0.080374	0.11	0.63398	0.13	0.05721	0.05	498.4	0.6	498.6	0.6	498.6	1.0	0.927
	5	0.00032	36.1	0.3	164.9	1160.1	0.05	0.080351	0.09	0.63350	0.12	0.05718	0.07	498.2	0.4	498.3	0.6	497.5	1.6	0.804
Mean		Recommended values						0.080422	0.01	0.63388	0.03	0.05717	0.003	498.7	0.4	498.5	0.5	497.2	1.2	

[a] (1) $^{206}Pb/^{204}Pb$ for mass spectrometric measurement; $^{206}Pb/^{238}U$, $^{207}Pb/^{235}U$, and $^{207}Pb/^{206}Pb$ for blank, initial Pb and mass fractionation correction. (2) $\lambda_{238} = 1.55125 \times 10^{-10}$ and $\lambda_{235} = 9.8485 \times 10^{-10}$ (Jaffey *et al.*, 1971);[34] $^{238}U/^{235}U = 137.818$ (Hiess *et al.*, 2012).[35] (3) Pb for total Pb, and Pb_c for measurement of common Pb. (4) Common Pb subtraction using the Stacey and Kramers (1975)[27] model. (5) 13 pg Pb and 1 pg U for total procedure blank.

Table 4 Compilation of ID-TIMS U–Pb or LA-Q/SF-ICP-MS age of Xtm-NHBS, BS-1, MG-1 and XN Datas xenotimes for *in situ* U–Pb geochronology[a]

				Data for the Wetherill plot						Apparent dates (Ma)						
Samples	No.	Methods	n	$^{207}Pb/^{206}Pb$	1s	$^{207}Pb/^{235}U$	1s	$^{206}Pb/^{238}U$	1s	$^{207}Pb/^{206}Pb$	1s	$^{207}Pb/^{235}U$	1s	$^{206}Pb/^{238}U$	1s	References
		ID-TIMS	5							497.2	1.2	498.5	0.5	498.7	0.4	This study
	* 1	LA-Q-ICP-MS	23	0.0574	0.0011	0.631	0.011	0.0798	0.0011	513	31	496.7	6.9	494.9	6.7	This study
	* 2	LA-SF-ICP-MS	24	0.0571	0.0009	0.637	0.011	0.0809	0.0008	496	33	500.5	6.7	501.3	4.8	This study
Xtm-NHBS	* 3	LA-SF-ICP-MS	27	0.0575	0.0010	0.633	0.010	0.0798	0.0010	512	21	497.7	6.0	494.7	5.9	This study
	* 4	LA-SF-ICP-MS	28	0.0569	0.0008	0.633	0.013	0.0808	0.0013	485	27	497.9	8.3	500.6	7.7	This study
	* 5	LA-Q-ICP-MS	22	0.0575	0.0006	0.637	0.010	0.0807	0.0007	494	8	499.7	2.1	500.0	2.1	This study
	* 6	LA-Q-ICP-MS	24	0.0573	0.0007	0.641	0.010	0.0807	0.0004	475	11	501.5	3.2	499.0	2.0	This study
BS-1		ID-TIMS								505.5	0.6	508.2	0.6	508.9	0.3	3
BS-1	# 1	LA-SF-ICP-MS	34	0.0576	0.0008	0.652	0.007	0.0822	0.0006	504	14	510.0	4.5	509.4	3.8	This study
MG-1		ID-TIMS								491.8	0.3	490.4	0.3	490.0	0.3	3
MG-1	# 2	LA-SF-ICP-MS	49	0.0570	0.0004	0.620	0.005	0.0789	0.0006	491	10	489.9	3.3	489.5	3.3	This study
XN01		ID-TIMS								514.8	0.7	513.7	0.3	513.4	0.2	15
XN02		ID-TIMS								517.0	1.0	515.7	0.3	515.4	0.1	15
XN Datas	# 1	LA-SF-ICP-MS	30	0.0579	0.0006	0.656	0.009	0.0822	0.0010	526	18	512.1	5.7	509.2	6.2	This study
XN Datas	# 2	LA-SF-ICP-MS	30	0.0577	0.0007	0.656	0.010	0.0824	0.0010	520	18	512.2	6.2	510.4	6.0	This study

[a] Considering the high precision isotopic ratio obtained by ID-TIMS, only the U–Pb age is present for comparison. * means BS-1 as an external primary xenotime reference material. # means Xtm-NHBS as a primary xenotime reference material.

3. Results and discussion

In this study, the major and trace elements of Xtm-NHBS, BS-1, MG-1 and XN Datas xenotime samples are summarised in Tables 1 and 2 (see Table 1S†). The ID-TIMS U–Pb analytical results for Xtm-NHBS xenotime are presented in Table 3. For comparison, Table 4 compiled our obtained U–Pb data for available xenotime reference materials (*e.g.* BS-1, MG-1, and XN Datas) and the Xtm-NHBS sample in different analytical sessions using Q/SF-ICP-MS (see Tables 2S and 3S†).

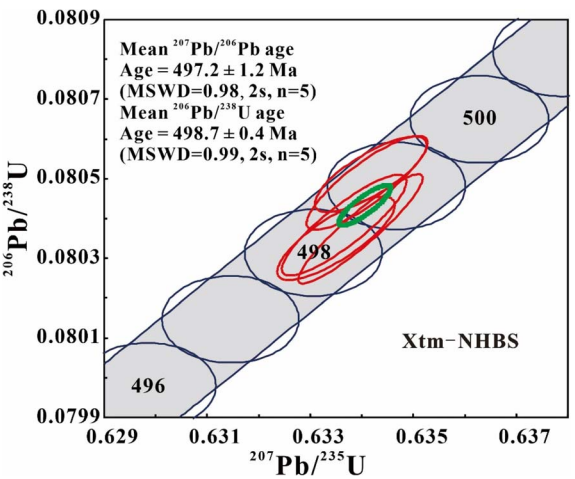

Fig. 2 Concordia U–Pb diagrams for ID-TIMS data of Xtm-NHBS xenotime samples and U–Pb ages calculated using Isoplot (Ludwig, 2003). Error ellipses represent 2 s uncertainties. The gray area is the concordia curve including the decay constant uncertainty by Jaffey *et al.* (1971). MSWD = mean square of weighted deviates.

Concordia diagrams of U–Pb data are plotted for all xenotime samples using the Isoplot 3.23 software package.[32] The ID-TIMS U–Pb analytical results for Xtm-NHBS xenotime are presented in Fig. 2. *In situ* U–Pb ages of the Xtm-NHBS xenotime samples are illustrated in Fig. 3 using LA-Q/SF-ICP-MS in different analytical sessions (see Table 2S†). In order to demonstrate the robustness and feasibility of Xtm-NHBS xenotime as a primary reference material, the *in situ* U–Pb ages of the BS-1, MG-1 and XN Datas xenotime are plotted in Fig. 4 (see Table 3S†). Duplicate *in situ* Lu–Hf ages of the Xtm-NHBS xenotime are illustrated in Fig. 5 using LA-ICP-MS/MS (see Table 4S†). Chondrite-normalised rare earth element (REE) data for BS-1, MG-1, XN Datas and Xtm-NHBS xenotimes are plotted in Fig. 6.[33] These data exhibit similar patterns and demonstrate a pronounced negative Eu anomaly, with the exception of some XN Datas samples (see Table 1S†).

3.1 ID-TIMS U–Pb measurement

Considering the limited availability of U–Pb xenotime reference materials (*i.e.*, BS-1 and MG-1), we selected the Xtm-NHBS xenotime sample for ID-TIMS U–Pb measurements based on

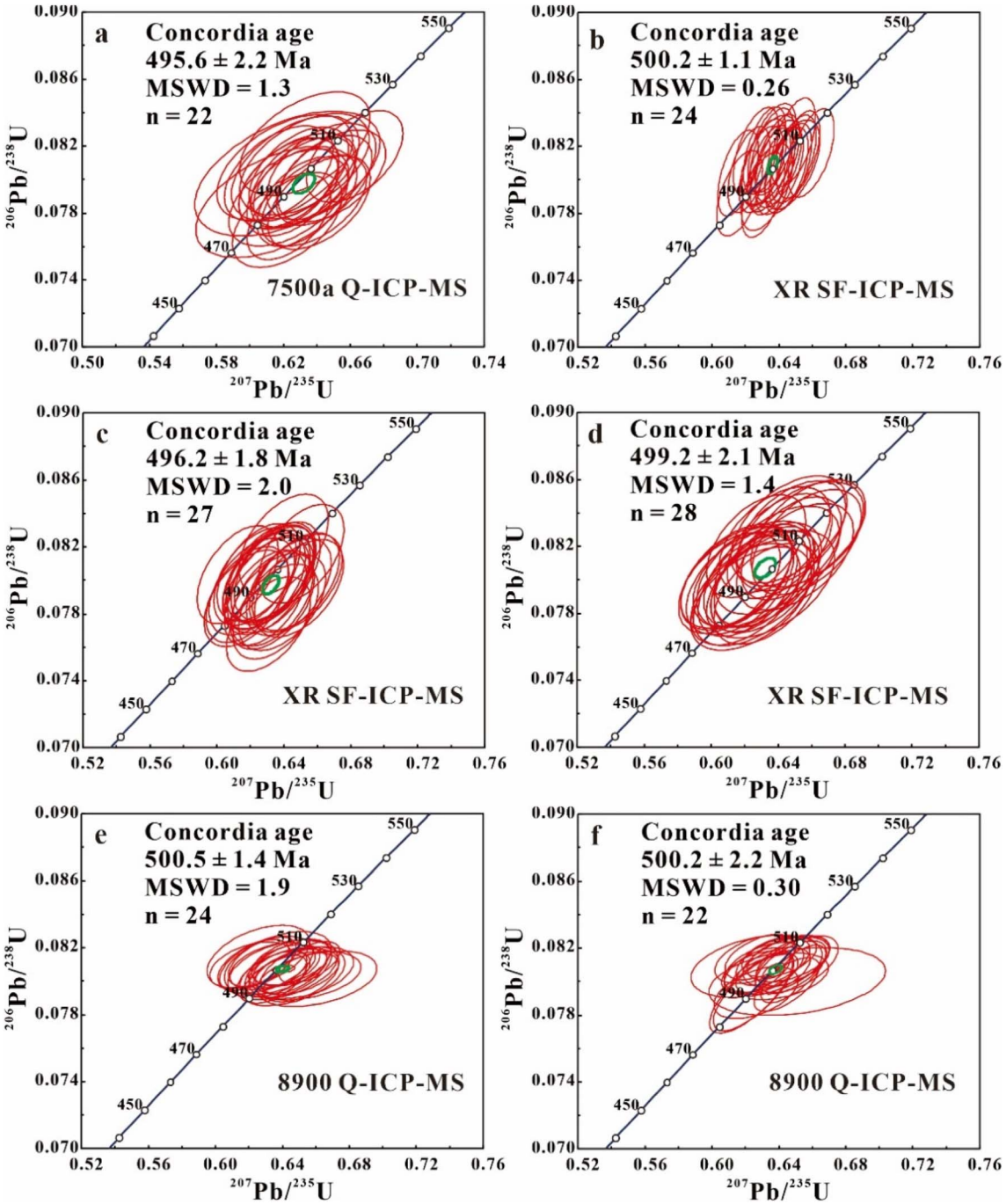

Fig. 3 The concordant U–Pb ages of Xtm-NHBS xenotime using LA-Q/SF-ICP-MS (7500a Q-ICP-MS (a), Element XR SF-ICP-MS (b–d), and 8900 Q-ICP-MS (e and f)). These data indicate that our obtained concordant U–Pb ages of Xtm-NHBS xenotime agree well with each other in different analytical sessions. MSWD = mean square of weighted deviates. Data were plotted and evaluated using Isoplot (Ludwig, 2003). Error bars in the insets are at the 1s level.

our multiple laser analyses. The Xtm-NHBS sample was chosen due to its low common Pb, high U contents, and trace element content without too many various ranges (Table 3). Five aliquots of the Xtm-NHBS xenotime were analysed by ID-TIMS in TJ-CGS. The measured $^{206}Pb/^{204}Pb$ ratios for the Xtm-NHBS sample range from 1132.3 to 1651.3. The total U contents vary between 164.9 μg g^{-1} and 206.1 μg g^{-1}. The U–Pb results are consistent within analytical uncertainty, yielding a weighted average $^{206}Pb/^{238}U$ and $^{207}Pb/^{235}U$ ages of 498.7 ± 0.4 Ma (2s, MSWD = 0.99) and 498.5 ± 0.5 Ma (2s, MSWD = 0.10), respectively. The weighted average $^{207}Pb/^{206}Pb$ age of 497.2 ± 1.2 Ma (2s, MSWD = 0.98) has a relatively large uncertainty (Fig. 2). Nevertheless, the $^{207}Pb/^{206}Pb$ age is usually an important indicator of homogeneity for *ca.* 500 Ma. A consistent $^{207}Pb/^{206}Pb$ ratio is suitable

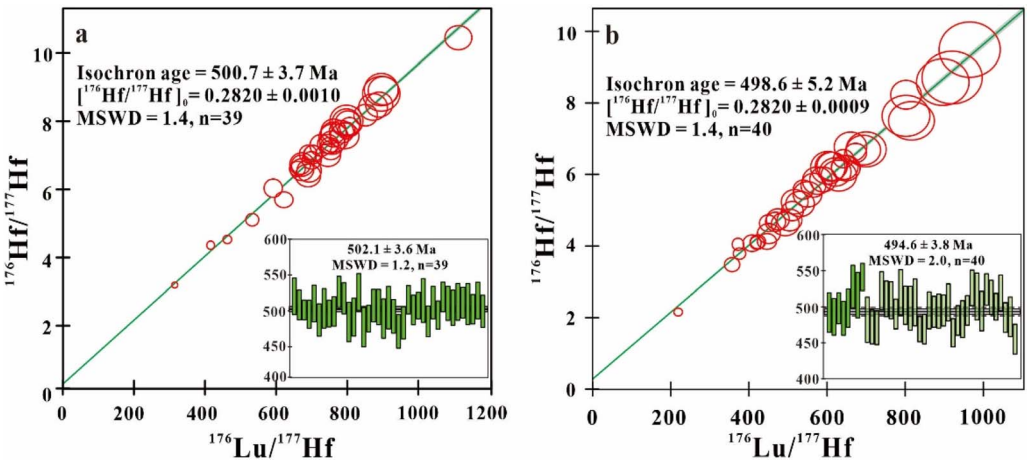

Fig. 4 The Lu–Hf isochron age plot and common Hf corrected single-spot Lu–Hf age of Xtm-NHBS xenotime using LA-ICP-MS/MS in two analytical sessions (a and b). These data indicate that Xtm-NHBS xenotime is a potential reference material for *in situ* Lu–Hf geochronology of xenotime. MSWD = mean square of weighted deviates. Error bars in the insets are at the 1s level.

for normalization despite the young age. These results demonstrate that Xtm-NHBS exhibits homogeneous U–Pb age and Pb–Pb age. Therefore, we recommend a concordia age of 498.7 ± 0.2 Ma (2s, MSWD = 0.7) as the U–Pb reference age for the Xtm-NHBS xenotime in the future (Table 4).

3.2 *In situ* U–Pb/Lu–Hf measurement

Our laser multiple analyses indicate that the Xtm-NHBS xenotime exhibits relatively homogeneous U values of approximately 150 μg g^{-1}, with a Th/U ratio of around 7.5 (Tables 2 and 2S†). During six laser analytical sessions, a total of twenty-two

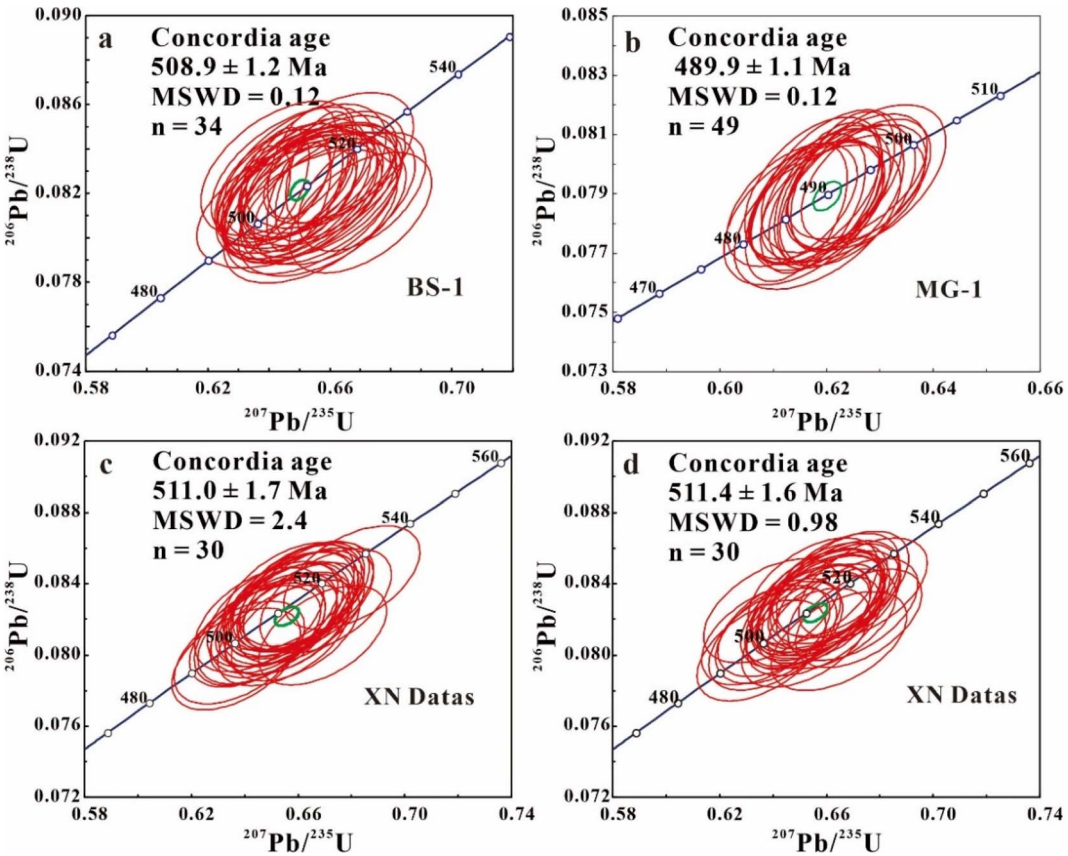

Fig. 5 The concordant U–Pb ages of BS-1 (a), MG-1 (b) and XN Datas (c and d) using Xtm-NHBS xenotime as the primary reference material by LA-SF-ICP-MS (Element XR). These data indicate that Xtm-NHBS xenotime is an excellent xenotime reference material for *in situ* U–Pb geochronology. MSWD = mean square of weighted deviates. Error bars in the insets are at the 1s level.

spots were measured using the 7500a Q-ICP-MS, yielding a concordia age of 495.6 ± 2.2 Ma (2s, MSWD = 1.3) (Fig. 3a). Three analyses using the Element XR SF-ICP-MS yielded the concordia ages: 500.2 ± 1.1 Ma (2s, n = 24, MSWD = 0.26), 496.2 ± 1.8 Ma (2s, n = 27, MSWD = 2.0), and 499.2 ± 2.1 Ma (2s, n = 28, MSWD = 1.4), respectively (Fig. 3b–d). Two analyses using the 8900 Q-ICP-MS yielded the concordia ages: 500.5 ± 1.4 Ma (2s, n = 24, MSWD = 1.9) and 500.2 ± 2.2 Ma (2s, n = 22, MSWD = 0.30), respectively (Fig. 3e and f). These *in situ* values obtained from LA-Q/SF-ICP-MS analyses are statistically consistent with the ID-TIMS U–Pb age, indicating the homogeneity of the Xtm-NHBS crystal.

Meanwhile, a total of seventy-nine spots were measured on Xtm-NHBS using LA-ICP-MS/MS during the two analytical sessions, yielding an isochron Lu–Hf age of 500.7 ± 3.7 Ma (2s, n = 39, MSWD = 1.4) and 498.6 ± 5.2 Ma (2s, n = 40, MSWD = 1.4), respectively. The weighted mean common Hf corrected single-spot Lu–Hf age is 502.1 ± 3.6 Ma (2s, n = 39, MSWD = 1.2), 494.6 ± 3.8 Ma (2s, n = 40, MSWD = 2.0), respectively (Fig. 5a and b). These *in situ* Lu–Hf ages obtained using LA-ICP-MS/MS are also in good agreement with the U–Pb age, indicating the homogeneity of the Xtm-NHBS crystal and potential reference material for *in situ* Lu–Hf geochronology.

3.3 Xtm-NHBS reference materials for *in situ* U–Pb/Lu–Hf geochronology

For comparison, the available xenotime reference materials including BS-1, MG-1, Xn Data and Xtm-NHBS for *in situ* U–Pb dating are summarised in Table 4. As the main *in situ* U–Pb reference materials, BS-1 and MG-1 xenotimes have been widely used since 2004, but are now almost consumed in SIMS or LA-(MC)-ICP-MS laboratories and have become unavailable,

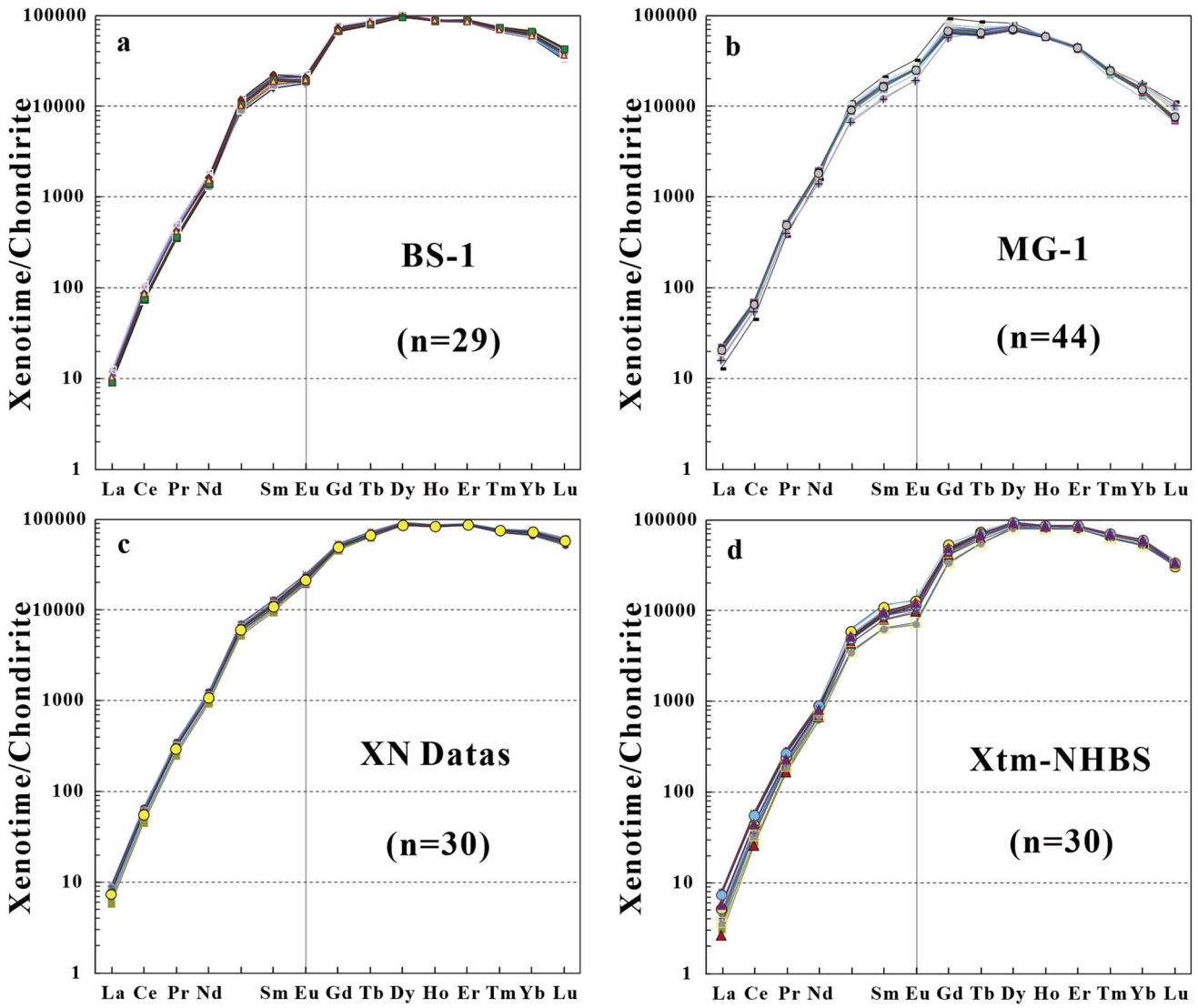

Fig. 6 The chondrite-normalized REE distribution patterns of BS-1 (a), MG-1 (b), XN Datas (c) and Xtm-NHBS (d) reference materials in this work. Concentrations were normalized using the chondrite values from McDonough and Sun (1995).

especially for laser colleagues. The new reference material, XN Datas xenotime, has recently been introduced, though its homogeneity needs interlaboratory evaluation in the future.[15] In this study, to validate the robustness and reliability of Xtm-NHBS xenotime as a primary reference material, we conducted tests on the xenotime samples of BS-1, MG-1, and XN Datas using Xtm-NHBS as the external standard. The results are presented in Fig. 4 (see Table 3S†).

Fig. 4a and b show the U–Pb ages obtained for BS-1 and MG-1 during the same analytical sessions, yielding concordia ages of 508.9 ± 1.2 Ma (2s, MSWD = 0.12, $n = 34$) and 489.9 ± 1.1 Ma (2s, MSWD = 0.12, $n = 49$), respectively. These results are consistent with the recommended ages for BS-1 (508.9 ± 0.3 Ma, ID-TIMS) and MG-1 (490.0 ± 0.3 Ma, ID-TIMS) within the analytical uncertainty. The weighted mean $^{206}Pb/^{238}U$ ages were 509.5 ± 3.6 Ma (2s, $n = 34$) and 489.5 ± 2.8 Ma (2s, $n = 49$), respectively (Table 4). Meanwhile, Fig. 4c and d display the U–Pb dating results obtained for XN Datas as unknown samples during the two analytical sessions using Xtm-NHBS as the primary standard. The two sessions yielded concordia ages of 511.0 ± 1.7 Ma (2s, MSWD = 2.4, $n = 30$) and 511.4 ± 1.6 Ma (2s, MSWD = 0.98, $n = 30$), which align with the ID-TIMS $^{206}Pb/^{238}U$ ages (513.4 ± 0.5 Ma, 515.4 ± 0.2 Ma), with a deviation of less than 1% (Table 4). The weighted mean $^{206}Pb/^{238}U$ ages from the two sessions were 509.0 ± 4.1 Ma (2s, $n = 30$) and 510.4 ± 4.0 Ma (2s, $n = 30$), respectively (Table 4).

Moreover, as mentioned above, the rapid development of LA-ICP-MS/MS has increased demand for xenotime reference materials suited for *in situ* Lu–Hf dating.[20–22] Xtm-NHBS xenotime exhibits a relatively high Lu/Hf ratio of ~600 as well as 1200 μg g^{-1} Lu and ~2 μg g^{-1} Hf, indicating an ideal object for *in situ* Lu–Hf dating of U–Pb reference materials (*e.g.*, BS-1 and XN Datas). Our duplicate *in situ* Lu–Hf measurement also demonstrated the consistency between Lu–Hf and U–Pb ages (Fig. 4, see in Table 3S†).[22]

In summary, the U–Pb dating results obtained for BS-1, MG-1, and XN Datas using Xtm-NHBS as the primary reference material are consistent with the ID-TIMS results within the analytical uncertainty (Table 4). This demonstrates the reliability and homogeneity of the Xtm-NHBS crystal, making it a suitable primary U–Pb/Lu–Hf geochronology reference material. With the accumulation of analytical data, Xtm-NHBS xenotime will likely become a viable choice as a supply of BS-1, MG-1, and XN Datas reference materials in the future.

4. Conclusions

U–Pb ages of the Xtm-NHBS xenotime were measured multiple times in this study, and its chemical composition was characterised for evaluation as a potential primary reference material in U–Pb geochronology. The ID-TIMS $^{206}Pb/^{238}U$ age of 498.7 ± 0.4 Ma (2s, $n = 5$) for Xtm-NHBS is interpreted as the crystallisation age of this metacyst and is recommended as the preferred age for the primary reference material. U–Pb isotopic analyses were conducted using both ID-TIMS and LA-Q/SF-ICP-MS to examine the homogeneity of the xenotime gem-quality crystals. Additionally, the ages of BS-1, MG-1, and XN Datas can be reproduced when calibrated against the Xtm-NHBS crystal and the Lu–Hf ages of this crystal by LA-ICP-MS/MS are also presented in this work and are also in good agreement with the U–Pb age. This newly characterised natural Xtm-NHBS xenotime reference material is expected to significantly contribute to the rapid advancement of *in situ* U–Pb/Lu–Hf geochronology, enhancing both accuracy and precision in microanalytical applications.

Data availability

The data that support the findings of this study are available in the ESI† of this article. Crystals and fragments of Xtm-NHBS are available upon request for colleagues by contacting Y. H. Yang (yangyueheng@mail.iggcas.ac.cn).

Author contributions

Formal analysis, S. Y. Zhang, L. Xu, J. R. Tu and C. Huang; conceptualization, Y. Y. Yang; methodology, S. T. Wu.; writing–original draft, S. Y. Zhang and Y. H. Yang; review, H. Wang, L. W. Xie, J. H. Yang, F. Y. Wu; funding acquisition, Y. H. Yang.

Conflicts of interest

There are no conflicts to declare.

Acknowledgements

This work was financially supported by the Natural Science Foundation of China (42430105, 42473037 and 42173035), the State Key Laboratory of Lithospheric and Environmental Coevolution (SKL-Z202304) and the Key Research Program of the Institute of Geology and Geophysics, Chinese Academy of Sciences (IGGCAS-202301). We are indebted to Shaohua Zhang, Junlong Niu and Yijia Wang for mass spectrometric measurement and Bohang Xie for sample preparation. We would like to thank Ryan Ickert (Purdue University) and an anonymous reviewer for helpful comments, as well as Emma Stephen for efficient handling during submission.

References

1 Z. C. Liu, F. Y. Wu, C. L. Guo, Z. F. Zhao, J. H. Yang and J. F. Sun, *Chin. Sci. Bull.*, 2011, **56**, 2948–2956.
2 N. J. McNaughton, B. Rasmussen and I. R. Fletcher, *Science*, 1999, **285**, 78–80.
3 R. Fletcher, B. Rasmussen and N. J. McNaughton, *Austin J. Earth Sci.*, 2000, **47**, 845–859.
4 R. A. Stern and N. Rayner, *Radiogenic Age and Isotopic Studies: Report 16, Geological Survey of Canada, Current Research*, 2003, 2003–F1, pp. 1–7.
5 B. Rasmussen, *Earth-Sci. Rev.*, 2005, **68**, 197–243.
6 J. N. Aleinikoff, R. I. Grauch, F. K. Mazdab, L. Kwak, C. M. Fanning and S. L. Kamo, *Am. J. Sci.*, 2012, **312**, 723–765.
7 J. Cross and I. S. Williams, *Chem. Geol.*, 2018, **484**, 81–108.

8 Q. L. Li, X. H. Li, Z. W. Lan, C. L. Guo, Y. N. Yang, Y. Liu and G. Q. Tang, *Contrib. Mineral. Petrol.*, 2013, **166**, 65–80.

9 T. Luo, H. Zhao, Q. L. Li, Y. Li, W. Zhang, J. L. Guo, Y. S. Liu, J. F. Zhang and Z. C. Hu, *Geostand. Geoanal. Res.*, 2020, **44**, 653–668.

10 T. Luo, H. Zhao, W. Zhang, J. L. Guo, K. Zong, Y. S. Liu, J. Zhang and Z. C. Hu, *Sci. China:Earth Sci.*, 2021, **64**, 667–676.

11 Y. H. Yang, F. Y. Wu, J. H. Yang, R. H. Mitchell, Z. F. Zhao, L. W. Xie, C. Huang, Q. Ma, M. Yang and H. Zhao, *J. Anal. At. Spectrom.*, 2018, **33**, 231–239.

12 Y. H. Yang, F. Y. Wu, Q. L. Li, Y. Rojas-Agramonte, J. H. Yang, Y. Li, Q. Ma, L. W. Xie, C. Huang, H. R. Fan, Z. F. Zhao and C. Xu, *Geostand. Geoanal. Res.*, 2019, **43**, 543–565.

13 M. Yang, Y. H. Yang, S. T. Wu, R. L. Romer, X. D. Che, Z. F. Zhao, W. S. Li, J. H. Yang, F. Y. Wu, L. W. Xie, C. Huang, D. Zhang and Y. Zhang, *J. Anal. At. Spectrom.*, 2020, **35**, 2191–2203.

14 Y. H. Yang, M. Yang, H. Wang, J. H. Yang and F. Y. Wu, *Sci. China:Earth Sci.*, 2021, **64**, 187–190.

15 D. Vasconcelos, G. O. Gonçalves, C. Lana, I. S. Buick, S. L. Kamo, F. Corfu, R. Scholz, A. Alkmim, G. Queiroga and H. A. Nalini, *Geochem., Geophys., Geosyst.*, 2018, **19**, 2262–2282.

16 S. T. Wu, M. Yang, Y. H. Yang, L. W. Xie, C. Huang, H. Wang and J. H. Yang, *Int. J. Mass Spectrom.*, 2020, **456**, 116394.

17 S. T. Wu, Y. H. Yang, N. M. W. Roberts, M. Yang, H. Wang, Z. W. Lan, T. Y. Li, L. Xu, C. Huang, L. W. Xie, J. H. Yang and F. Y. Wu, *Sci. China:Earth Sci.*, 2022, **65**, 1146–1160.

18 Y. H. Yang, S. T. Wu, H. Wang, S. L. Kamo, Q. Ma, T. Liang, L. Xu, L. W. Xie, C. Huang, J. H. Yang and F. Y. Wu, *J. Anal. At. Spectrom.*, 2025, **40**, 326–337.

19 R. Fletcher, N. J. McNaughton, J. A. Aleinikoff, B. Rasmussen and S. L. Kamo, *Chem. Geol.*, 2004, **209**, 295–314.

20 T. Zack and J. Hogmalm, *Goldschmidt*, Prague, Czech Republic, 2015, p. 3557.

21 A. Simpson, S. Gilbert, R. Tamblyn, M. Hand, C. Spandler, J. Gillespie, A. Nixon and S. Glorie, *Chem. Geol.*, 2021, **577**, 120299.

22 S. T. Wu, H. Wang, Y. H. Yang, J. L. Niu, Z. W. Lan, L. L. Zhang, C. Huang, L. W. Xie, L. Xu, J. H. Yang and F. Y. Wu, *J. Anal. At. Spectrom.*, 2023, **38**, 1285–1300.

23 S. T. Wu, G. Woerner, K. P. Jochum, B. Stoll, K. Simon and A. Kronz, *Geostand. Geoanal. Res.*, 2019, **43**, 567–584.

24 J. R. Tu, Z. B. Xiao, H. Y. Zhou, S. Q. An, G. Z. Li, Y. R. Cui, W. G. Liu and H. M. Li, *Ore Geol. Rev.*, 2019, **109**, 407–412.

25 R. A. Stern and N. Rayner, *Current Research*, 2003, **Fl**, 1–7.

26 D. J. Condon, B. Schoene, M. Schmitz, U. Schaltegger, R. B. Ickert, Y. Amelin, L. E. Augland, K. R. Chamberlain, D. S. Coleman, J. N. Connelly, F. Corfu, J. L. Crowley, J. H. F. L. Davies, S. W. Denszyn, M. P. Eddy, S. P. Gaynor, L. M. Heaman, M. H. Huyskens, S. Kamo, J. Kasbohm, C. B. Keller, S. A. Maclennan, N. M. McLean, S. Noble, M. Ovtcharova, A. Paul, J. Remezani, M. Rioux, D. Sahy, J. S. Scoates, D. Szymanowski, S. Tapster, M. Tichomirowa, C. J. Wall, J. F. Wotzlaw, C. Yang and Q. Z. Yin, *GSA Bulletin*, 2024, **136**, 4233–4251.

27 J. S. Stacey and J. D. Kramers, *Earth Planet. Sci. Lett.*, 1975, **26**, 207–221.

28 S. T. Wu, Y. H. Yang, H. Wang, C. Huang, L. W. Xie and J. H. Yang, *At. Spectrosc.*, 2020, **41**, 154–161.

29 M. Yang, R. L. Romer, Y. H. Yang, S. T. Wu, H. Wang, J. R. Tu, H. Y. Zhou, L. W. Xie, C. Huang, L. Xu, J. H. Yang and F. Y. Wu, *Chem. Geol.*, 2022, **593**, 120754.

30 S. T. Wu, J. L. Niu, Y. H. Yang, H. Wang, J. H. Yang and F. Y. Wu, *J. Anal. At. Spectrom.*, 2024, **39**, 2703–2715.

31 S. T. Wu, Y. H. Yang, H. Wang, N. M. W. Roberts, J. L. Niu, Y. J. Wang, J. H. Yang and F. Y. Wu, *Chem. Geol.*, 2024, **670**, 122383.

32 K. R. Ludwig, *ISOPLOT 3.0: A Geochronological Toolkit for Microsoft Excel*, Berkeley Geochronology Center, Special Publication, 2003, vol. 4, p. 71.

33 W. F. McDonough and S. S. Sun, *Chem. Geol.*, 1995, **120**(3–4), 223–253.

34 A. H. Jaffey, K. F. Flynn, L. E. Glendenin, W. C. Bentley and A. M. Essling, *Phys. Rev.*, 1971, **4**, 1889–1906.

35 J. Hiess, D. J. Condon D.J., N. McLean and S. R. Noble, *Science*, 2012, **335**(6076), 1585–1586.